

Ablation and Thermal Properties of Ethylene–Propylene–Diene Elastomer Composites Reinforced with Polysulfonamide Short Fibers

Xiaolong Jia, Gang Li, Yunhua Yu, Gang Sui, Haiyang Liu, Ya'nán Li, Peng Li, Xiaoping Yang

Key Laboratory of Beijing City on the Preparation and Processing of Novel Polymer Materials, Beijing University of Chemical Technology, Beijing 100029, People's Republic of China

Received 8 July 2008; accepted 21 August 2008

DOI 10.1002/app.29470

Published online 19 March 2009 in Wiley InterScience (www.interscience.wiley.com).

ABSTRACT: Polysulfonamide (PSA) short fiber/ethylene–propylene–diene elastomer (EPDM) composites were prepared as high-performance thermal insulators. The pyrolysis products and thermal stabilities of the PSA fiber and aramid fiber were analyzed. The ablation and thermal properties of the PSA/EPDM composites were compared with those of the aramid/EPDM composites. The degradation peak temperature of the PSA fiber was 100°C higher than that of the aramid fiber. With the fiber content increasing, the ablation rates of both composites decreased up to 10 phr and subsequently increased, whereas the thermal conductivities of both composites increased linearly. In comparison with the

aramid/EPDM composites, the ablation rate and thermal conductivity of the PSA/EPDM composites were lower, whereas the thermal degradation temperature and limiting oxygen index of the PSA/EPDM composites were higher. Dynamic mechanical thermal testing and morphology observations revealed that strong interfacial bonding between the fiber and the matrix was developed in the PSA/EPDM composites, and it was beneficial for improving the ablation properties of the composites. © 2009 Wiley Periodicals, Inc. *J Appl Polym Sci* 113: 283–289, 2009

Key words: composites; morphology; thermal properties

INTRODUCTION

Thermal insulators, used as heat-barrier materials between the case and the propellant, are essential components of rocket motors, and they have good thermal resistance and good ablation properties.^{1–4} Various fiber-reinforced elastomer composites are used as thermal insulators.^{5–8} Among the fiber-reinforced elastomer composites, ethylene–propylene–diene elastomer (EPDM) composites are the most favored because of their advanced properties, such as excellent ablation properties and low specific gravity.^{5,9–12} However, with the fast development of rocket motor technologies, high-performance thermal insulators are required to endure the severe conditions of high-temperature combustion gases.^{3,13,14} At present, aramid fiber has been widely applied as a reinforcing material to improve the performance of EPDM thermal insulators in various rocket motors.^{8,15–18} Recently, polysulfonamide (PSA) fiber, with a chemical structure similar to that of aramid fiber, has emerged as a new reinforcing material with the advantages of low cost and rich resources.¹⁹ Moreover, PSA fiber has exhibited excellent proper-

ties in EPDM composites²⁰ and could further improve the performance of these composites. However, there have been few reports on EPDM composites reinforced with PSA fiber up to now, especially with respect to the ablation and thermal properties of thermal insulators.

Therefore, the purpose of this study was the investigation of the ablation and thermal properties of EPDM composites reinforced with PSA short fiber. To this end, (1) the pyrolysis and derivative thermogravimetry (DTG) analysis of PSA fiber and aramid fiber were carried out to investigate the degradation performance and thermal stabilities; (2) PSA/EPDM composites and aramid/EPDM composites were prepared under their optimum conditions; and (3) the ablation properties, thermal conductivity, thermal stability, flame retardancy, dynamic mechanical thermal properties, and morphology of the PSA/EPDM composites were characterized, and the results were compared with those of the aramid/EPDM composites.

EXPERIMENTAL

Composite preparation

The materials used in this study were EPDM (J-3035, Jilin Chemical Co., Jilin, China), liquid EPDM, nano-silica, additives, and curing agents with a weight

Correspondence to: X. Yang (yangxp@mail.buct.edu.cn).

ratio of 100 : 15 : 20 : 15 : 13.6. The curing agents were composed of sulfur, zinc oxide, stearate acid, 2-sulfonyl dibenzothiazole, and diphenyl guanidine with a weight ratio of 2.5 : 4 : 2 : 3.6 : 1.5; this conformed with our previous work.²⁰ The contents of the PSA short fiber (0.5–3 mm) or aramid short fiber (0.5–3 mm) were adjusted to 0, 5, 10, 15, and 20 parts per hundred grams (phr) of EPDM. All materials were mixed uniformly at 50°C with an internal mixer (Rheocord 90, Haake Mess-Technic GmbH, Goettfert, Germany) at a speed of 100 rpm for 10 min. Then, the mixture was passed through a two-roll mill (XK-560, Dalian Huari Machine Co., Dalian, China) at a speed ratio of 1/1.1. The composite plaques were obtained through the molding of the mixture with iron frames of 3- and 10-mm thicknesses at 160°C under the pressure of 10 MPa for the optimum curing time. The optimum curing time was determined with a rheometer (P3555B2, Beijing Huanfeng Chemical Machine Co., Beijing, China) in advance. The chemical structures of the PSA fiber and the aramid fiber are shown in Figure 1(a,b).

Pyrolysis and DTG analysis

Pyrolysis analysis of the PSA fiber and aramid fiber was carried out to investigate the degradation performance of the fibers on a gas chromatography/mass spectrometry instrument (GCMS-QP5050A, Shimadzu, Europe, Duisburg, Germany) with a PYR-4A pyrolyzer consisting of a heated interface, a platinum coil probe, a quartz sample tube, and an electronic control module. The electron ionization source was under 70 eV, and a 30 m × 0.25 mm (inner diameter) fused silica capillary column (DB-5, Frontier) was used. The experimental conditions were set as close as possible to actual service conditions: a pyrolysis set temperature of 750°C, a pyrolysis interval of 30 s, a heating rate of 20°C/ms, an interface temperature of 280°C, a column temperature programmed from 50 (1 min) to 280°C (20 min) at 5°C/min, a splitting ratio of 30 : 1, a carrier gas (He) flow rate of 30 mL/min, a hydrogen pressure of 200 kPa, and an air pressure of 300 kPa. Samples of 3–5 mg were used.

The DTG analysis of the fibers and EPDM composites was performed with a TA Instrument Netzsch (Selb, Germany) STA 449C apparatus under an argon atmosphere at a purge rate of 40 mL/min. The samples were heated at a rate of 10°C/min. Samples of 10–12 mg were used.

Measurement of the ablation properties

Ablation testing was conducted on an YS22 oxyacetylene ablation tester (Xi'an Tianguan Scientific Co., Ltd., Xi'an, China) in accordance with ASTM E 285.

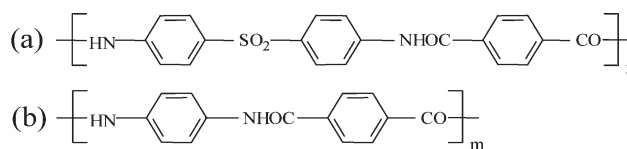


Figure 1 Chemical structures of the (a) PSA and (b) aramid fibers.

The composite plaques, 10 mm thick, were cut into round ablation specimens with a 30-mm diameter.

Measurement of the thermal conductivity and limiting oxygen index (LOI)

The thermal conductivity was measured on a thermal conductance tester (QTM-500, KEM Co., Kyoto, Japan) according to ASTM C 177. The composite plaques, 10 mm thick, were cut into round, thermally conductive specimens with a 30-mm diameter.

LOI was measured on an LOI tester (MDR 2000, Toyoseiki Co. Ltd., Kyoto, Japan) according to ASTM D 2863. One gram of the fibers was twisted on a metal wire with a 150-mm length and a 1-mm diameter. The composite plaques, 3 mm thick, were cut into rectangular specimens (100 × 6.5 mm²).

Dynamic mechanical thermal analysis

Dynamic mechanical thermal analysis was performed in a single-cantilever bending mode (DMTA-V, Rheometrics Scientific Co., USA). The specimen dimensions were 30 mm × 10 mm × 2 mm. The heating rate was 5°C/min from –100 to 100°C, and the fixed frequency was 1 Hz.

Morphology observation

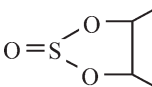

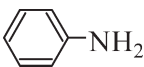
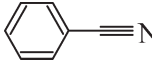
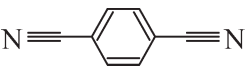
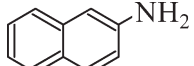
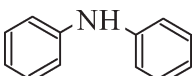
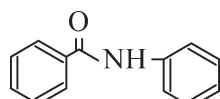
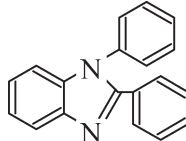
Morphologies of char layers and tensile fracture surfaces of EPDM composites were observed with scanning electron microscopy (S4700, Hitachi Co., Tokyo, Japan). The composite specimens were coated with a thin layer of a gold alloy.

RESULTS AND DISCUSSION

Pyrolysis and DTG analysis of the fibers

Tables I and II show the principal identified pyrolysis products of the PSA fiber and aramid fiber, respectively. Because of their chemical structures, the pyrolysis products of the PSA fiber and aramid fiber were mainly composed of aromatic compounds, which were deposited to form much char on the surface of the thermal insulator during ablation.^{21,22} According to Foldi,²³ the actual ablation of a thermal insulator mainly depends on the char layer on the surface of the insulator. The aromatic compounds produced by the PSA fiber and aramid

TABLE I
Principal Identified Pyrolysis Products of the PSA Fiber

Peak no.	Retention time (min)	Compound	Structure	Total area (%)
1	1.91	1,3,2-Dioxathiolane-4,5-dimethyl-2-oxide		18.91
2	2.56	Benzene		18.47
3	8.49	Aniline		5.81
4	8.64	Benzonitrile		26.32
5	19.82	1,4-Benzene dicyanitrile		0.33
6	20.73	2-Naphthalene carbonitrile		1.52
7	27.12	Diphenylamine		2.86
8	35.34	Benzanilide		6.56
9	44.28	1,2-Diphenyl benzimidazole		0.49

fiber were about 62.36 and 66.07% in total area, respectively, and this indicated that the two kinds of fibers greatly contributed to the char formation on the surface of the composites. Their contributions to the char formation were comparable.


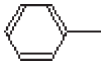
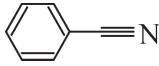
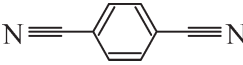
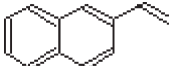
Figure 2 shows DTG curves of the PSA fiber and aramid fiber. The DTG curve of the aramid fiber slopes rapidly downward at 380°C and shows a peak at 474°C, whereas that of the PSA fiber slopes downward after 380°C and shows a peak at 574°C; this indicates that the thermal stability of the PSA fiber was much higher than that of the aramid fiber. This enhancement resulted from the existence of the additional sulfone ($-\text{SO}_2-$) group in the molecular

main chain of the PSA fiber. The sulfone group could act as a strong electron-withdrawing group because of the highest oxidation state of the element sulfur and conjugate with benzene rings of the molecular main chain.¹⁹ Therefore, the thermal stability of the PSA fiber was improved, and this could help to enhance the thermal insulation performance of the composites.

Ablation properties of the EPDM composites

Figure 3 shows the effects of the fiber content on the ablation rates of PSA/EPDM composites and aramid/EPDM composites. The ablation rates of both

TABLE II
Principal Identified Pyrolysis Products of the Aramid Fiber

Peak no.	Retention time (min)	Compound	Structure	Total area (%)
1	2.63	Benzene		38.43
2	3.64	Toluene		0.60
3	7.51	Benzonitrile		23.75
4	14.12	1,4-Benzene dicyanitrile		2.42
5	15.32	2-Ethenyl naphthalene		0.87

composites decreased with fiber contents up to 10 phr and then increased linearly. The initial decrease in the ablation rate could be explained by the enhancement of the thermal stability of the composites with the increase in the fiber content.¹ However, the tenacity of the char layer on the surface of the composites was greatly influenced by the fiber content, which dominated the adhesion between the char layer and virgin material. When the fiber content was high, that is, greater than 10 phr, the tenacity of the char layer on the surface of the composites decreased obviously.²⁴ During the intensive impingement of high-temperature combustion gases, the poor tenacity resulted in the fracturing and

sloughing of the formed char layer. Then, the underlying virgin material was exposed, and this led to the ablation rate increasing.

Figure 4 shows the morphologies of the char layers on the surfaces of PSA/EPDM composites and aramid/EPDM composites after ablation. A large number of ablated fibers were observed on the char layers of both composites. The arrows in Figure 4(a) show the ablated PSA short fiber, and the arrows in Figure 4(b) show the ablated aramid short fiber. The ablated PSA short fiber was rooted on the char layer and retained the char around it. In contrast, the ablated aramid short fiber just lay on the char layer and did not combine with the

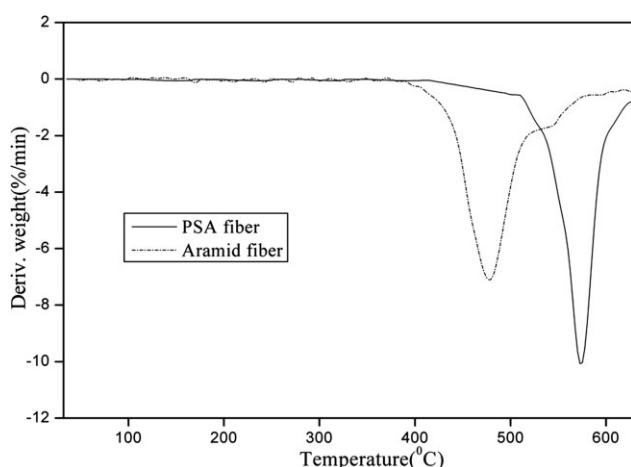


Figure 2 DTG curves of the PSA and aramid fibers.

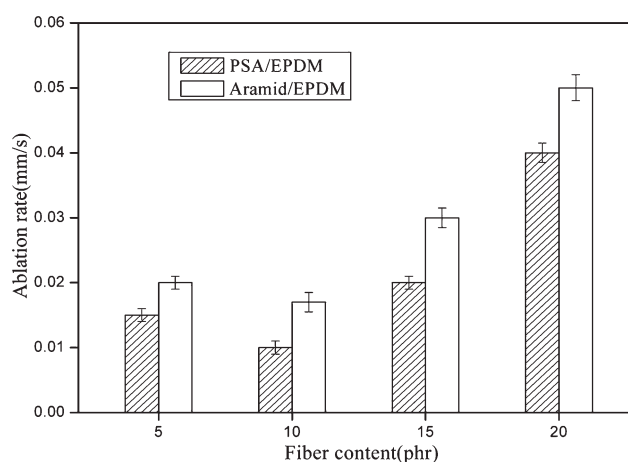


Figure 3 Effects of the fiber content on the ablation rates of the PSA/EPDM and aramid/EPDM composites.

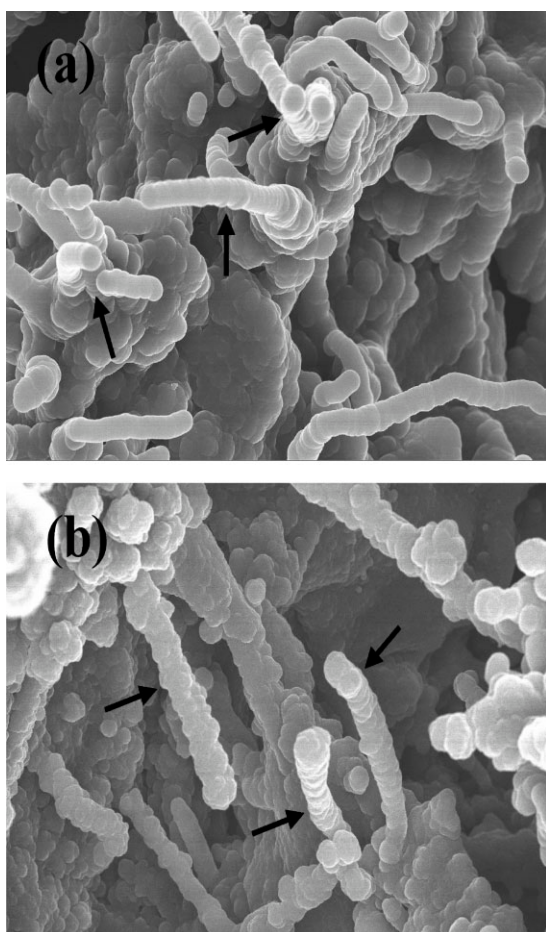


Figure 4 Morphologies of the char layers on the surfaces of the (a) PSA/EPDM and (b) aramid/EPDM composites after ablation.

surrounding char strongly; this was not beneficial for the ablation properties of the composites. Thus, the ablation rate of the PSA/EPDM composites, as shown in Figure 3, was obviously lower than that of the aramid/EPDM composites, and they showed better thermal insulation performance. Also, the difference in the ablation rate was related to the thermal conductivity, thermal stability, and flame retardancy of the composites as well as the interfacial bonding between the fiber and the matrix in the composites.

Thermal properties of the EPDM composites

The thermal conductivity, which is related to the steady-state temperature distribution, is an important parameter in estimating the effectiveness of heat transfer in materials.²⁵ Figure 5 shows the effects of the fiber content on the thermal conductivity of the PSA/EPDM composites and aramid/EPDM composites. With the fiber content increasing, the thermal conductivity of both composites increased. Similar results have been obtained with increasing contents

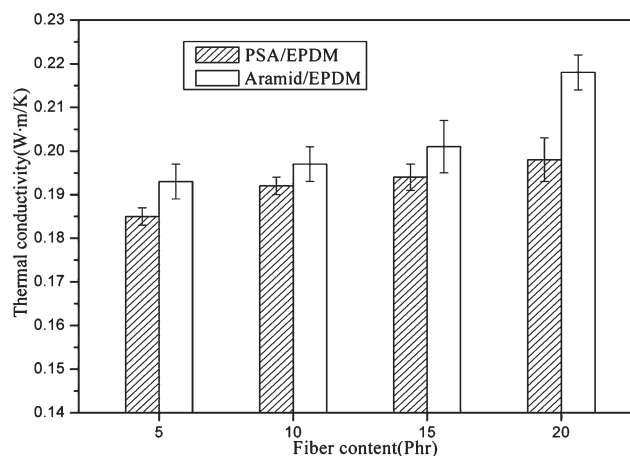


Figure 5 Effects of the fiber content on the thermal conductivity of the PSA/EPDM and aramid/EPDM composites.

of ceramic or carbon fillers.²⁶ The thermal conductivity of the PSA/EPDM composites was lower than that of the aramid/EPDM composites, and this showed that the heat was transferred more slowly in the PSA/EPDM composites than in the aramid/EPDM composites. The slower heat transfer indicated that more time was required to reach the degradation temperature of the composites, and this partly contributed to reducing material loss during ablation. Thus, the ablation rate of the PSA/EPDM composites was obviously lower than that of the aramid/EPDM composites, as shown in Figure 3.

Figure 6 shows the DTG curves of the EPDM composites with 10 phr short fiber. The DTG curve of the PSA/EPDM composites shows two peaks at 476 and 576°C, respectively, whereas that of the aramid/EPDM composites shows a sharp peak at 470°C; this indicates that the thermal stability of the PSA/EPDM composites was higher. According to Deuri

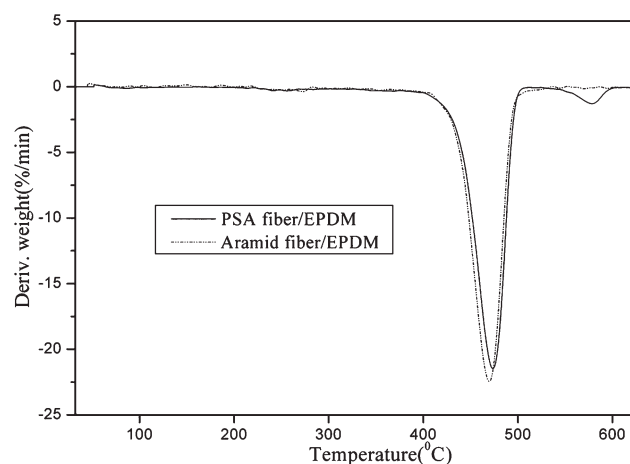


Figure 6 DTG curves of EPDM composites with 10 phr short fiber.

TABLE III
LOI Values of the Fibers and EPDM Composites
with 10 phr Short Fiber

	PSA fiber	Aramid fiber	PSA/ EPDM	Aramid/ EPDM
LOI	32.9 ± 0.4	27.7 ± 0.3	21.4 ± 0.3	20.6 ± 0.3

et al.,¹ the enhanced thermal stability of the composites was beneficial to the ablation properties.

Table III shows the LOI values of the fibers and EPDM composites with 10 phr short fiber. LOI is a parameter for evaluating the flame retardancy of materials. The LOI value of the PSA fiber was obviously higher than that of the aramid fiber, and this resulted in the improvement of the flame retardancy of the PSA/EPDM composites, as shown in Table III. According to Gan and Zhang,²⁷ higher flame retardancy of a thermal insulator can enhance its ablation properties.

Dynamic mechanical properties and morphologies of the EPDM composites

Figure 7 shows the storage modulus and $\tan \delta$ spectra of the EPDM composites with 10 phr short fiber. The interfacial bond strength in the composites was characterized by the energy dissipation that occurred in the polymer matrix and at the interface.²⁸ The stronger interface meant less energy dissipation, and this was in agreement with the higher storage modulus and lower $\tan \delta$ peak.^{29,30} The PSA/EPDM composites showed a higher storage modulus and a lower $\tan \delta$ peak than the aramid/EPDM composites, and this indicated stronger interfacial bonding between the fiber and the matrix in the PSA/EPDM composites, which was attributed to the sulfone group in the PSA fiber. The sulfone group attracted the electrons and reduced the electron cloud density of the amido group, and this decreased the polarity

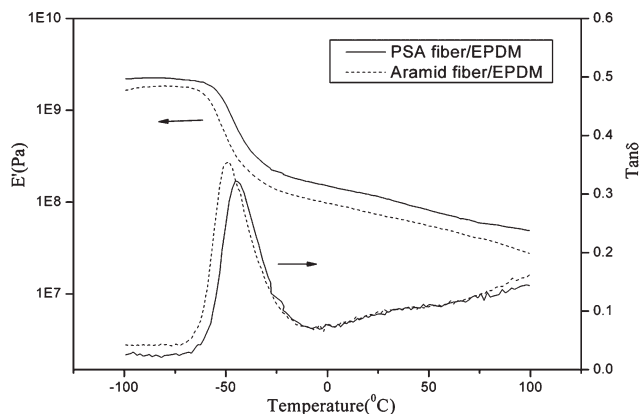


Figure 7 Storage modulus (E') and $\tan \delta$ spectra of the EPDM composites with 10 phr short fiber.

of the PSA fiber. The polarity of the PSA fiber was much lower than that of the aramid fiber. In addition, EPDM is a nonpolar polymer. Therefore, the compatibility of the PSA fiber and EPDM was better than that of the aramid fiber and EPDM, and this led to the stronger interfacial bonding between the fiber and the matrix in the PSA/EPDM composites.

Figure 8 shows the morphologies of the tensile fracture surfaces of the EPDM composites with 10 phr short fiber. In the PSA/EPDM composites, failure occurred primarily because of fiber breakage, whereas pulled-out fibers and holes left from pulled-out fibers were observed in the aramid/EPDM composites. PSA short fibers were seriously damaged by tensile fracture; however, the split and fibrillated fibers were still distributed in the matrix. Therefore, the effective bonding area was enlarged, and this resulted in an increase in the interfacial bonding between the fiber and the matrix in agreement with the analysis in Figure 7. However, aramid short

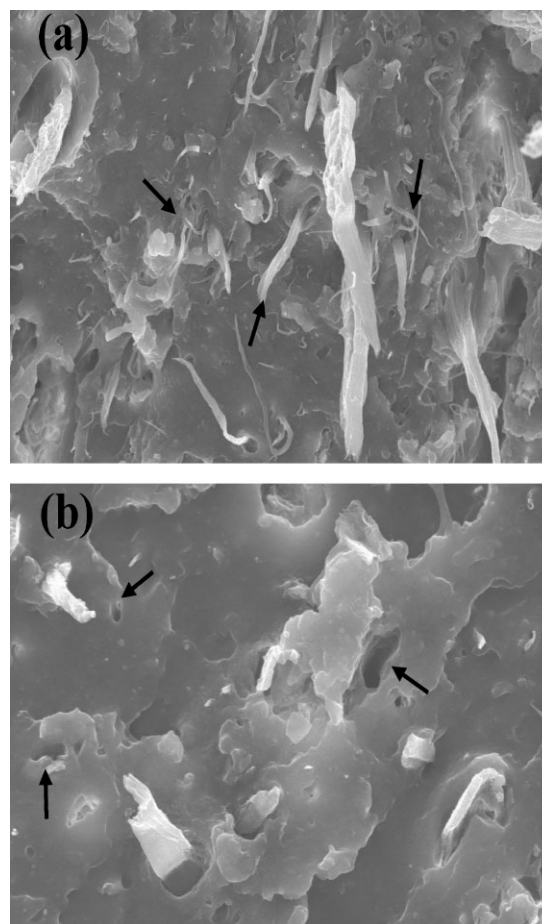


Figure 8 Morphologies of the tensile fracture surfaces of the EPDM composites with 10 phr short fiber: (a) PSA/EPDM and (b) aramid/EPDM composites. The arrows in part a show the breakage of the PSA short fibers, and the arrows in part b show the holes left from the pulled-out aramid short fibers.

fibers were extracted from the EPDM matrix, and this showed the weak interfacial bonding between the fiber and the matrix. The stronger interfacial bonding between the fiber and the matrix could enhance the ability of the short fiber to retain the surrounding char that formed on the surface of the composites during ablation, as shown in Figure 4(a). Foldi²³ reported that the actual ablation of a thermal insulator mainly depends on the char layer on the surface of the insulator. Therefore, the ablation properties of the PSA/EPDM composites were superior to those of the aramid/EPDM composites, as shown in Figure 3.

CONCLUSIONS

The thermal stability of the PSA fiber was much higher than that of the aramid fiber, although their contributions to the char formation were comparable. The ablation rate and thermal conductivity of the PSA/EPDM composites were lower than those of the aramid/EPDM composites, whereas the thermal degradation temperature and LOI of the PSA/EPDM composites were higher than those of the aramid/EPDM composites; this resulted in the improvement of the ablation properties of the PSA/EPDM composites. The excellent ablation properties were also due to stronger interfacial bonding between the fiber and the matrix in the PSA/EPDM composites. Therefore, in comparison with the aramid/EPDM composites, the PSA/EPDM composites exhibited superior potential as high-performance thermal insulators.

References

1. Deuri, A. S.; Bhowmick, A. K.; Ghosh, R.; John, B.; Sriram, T.; De, S. K. *Polym Degrad Stab* 1988, 21, 21.
2. Weisshaus, H.; Engleberg, I. *J Adv Mater* 1997, 28, 16.
3. Gao, Y. L.; Liang, G. Z.; Qiu, Z. M.; Liu, A. H. *Mater Lett* 2007, 61, 2406.
4. Rajeev, R. S.; De, S. K.; Bhowmick, A. K.; John, B. *Polym Degrad Stab* 2003, 79, 449.
5. Otto, G. *Solid Rocket Motor Internal Insulator*; National Aeronautics and Space Administration: Washington, DC, 1976; NASA SP-8093.
6. Nelson, D. S.; Prince, A. S. *AIAA/ASME/SAE/ASEE Joint Propulsion Conf* 1994, 30, 3184.
7. Parry, M. J. U.K. Pat. 2,295,396 (1996).
8. Guillot, D. G.; Harvey, A. R. U.S. Pat. 6,566,420 (2003).
9. Deuri, A. S.; Bhowmick, A. K. *Polym Degrad Stab* 1986, 16, 221.
10. Harvey, A. R.; Ellertson, J. W. U.S. Pat. 7,070,705 (2006).
11. Harvey, A. R.; Ellertson, J. W. U.S. Pat. 6,691,505 (2000).
12. Fitch, V.; Eddy, N. *AIAA/ASME/SAE/ASEE Joint Propulsion Conf* 1997, 33, 2992.
13. Huang, J. D.; Ye, D. Y. *Acta Astronaut* 1997, 40, 607.
14. Sureshkumar, M. S.; Bhuvaneswari, C. M.; Kakade, S. D.; Gupta, M. *Polym Adv Technol* 2008, 19, 144.
15. Fan, J. L. U.S. Pat. 6,953,823 (2005).
16. Jin, S.; Zheng, Y. S.; Gao, G. X.; Jin, Z. H. *Mater Sci Eng A* 2008, 483, 322.
17. Guillot, D. G. U.S. Pat. 6,893,597 (2005).
18. Harvey, A. R.; Ellertson, J. W. U.S. Pat. 6,606,852 (2000).
19. Wang, X. F.; Zhang, Y. H. *China Text Leader* 2005, 1, 19.
20. Jia, X. L.; Li, G.; Sui, G.; Li, P.; Yu, Y. H.; Liu, H. Y.; Yang, X. P. *Mater Chem Phys* 2008, 112, 823.
21. Youren, J. W. *Composites* 1971, 2, 180.
22. Herring, L. G. U.S. Pat. 4,878,431 (1989).
23. Foldi, A. P. *Short Fiber-Polymer Composites*; Woodhead: Cambridge, United Kingdom, 1996.
24. Zhang, J. S.; Lin, L.; Zhu, X. W. *J Solid Rocket Technol* 2002, 25, 38.
25. Tsai, I. J.; Lei, C. H.; Lee, C. H.; Lee, Y. C.; Lou, C. W.; Lin, J. H. *Mater Process Technol* 2007, 192, 415.
26. Uyarel, A. Y.; Pektas, I. *J Therm Anal* 1996, 46, 163.
27. Gan, X. X.; Zhang, S. J. *Explosives Propellants* 1994, 3, 1.
28. Rajeev, R. S.; Bhowmick, A. K.; De, S. K. *Polym Compos* 2002, 23, 574.
29. Rajeev, R. S.; Bhowmick, A. K.; De, S. K.; Bandyopadhyay, S. J. *Appl Polym Sci* 2003, 90, 554.
30. Rajeev, R. S.; Bhowmick, A. K.; De, S. K.; Bandyopadhyay, S. J. *Appl Polym Sci* 2003, 89, 1211.